Supporting information for

# Multi-proxy speleothem-based reconstruction of mid-MIS 3 climate in South Africa

Jenny Maccali[1,2], Anna Nele Meckler[1,2], Stein-Erik Lauritzen[1,2], Torill Brekken[3], Helen Aase Rokkan[3], Alvaro Fernandez[4], Yves Krüger[3], Jane Adigun[5], Stéphane Affolter[6], Markus Leuenberger[7]

[1]Department of Earth Sciences and Bjerknes Centre for Climate Research, University of Bergen, Bergen, N-5007, Norway
[2]SFF Centre for Early Sapiens Behaviour (SapienCE), University of Bergen, Bergen, N-5020, Norway
[3]Department of Earth Sciences, University of Bergen, Bergen, N-5007, Norway
[4]Andalusian Institute of Earth Sciences, University of Granada, Granada, 18100, Spain
[5]Department of Anthropology and Archaeology, University of South Africa, Pretoria, 0002, South Africa
[6]Department of Environmental Sciences, University of Basel, Basel, 4056, Switzerland
[7]Climate and Environmental Physics Division, Physics Institute and Oeschger Centre for Climate Change Research, University of Bern, Bern, 3012, Switzerland

## Supplement: dating performed at Xi'an Jiaotong University.

Additional $^{230}$Th dating of two samples was performed at the Isotope Laboratory, Xi'an Jiaotong University using multi-collector inductively coupled plasma mass spectrometers (MC-ICP-MS) (Thermo-Finnigan Neptune-*plus*). We used standard chemistry procedures to separate U and Th for dating (Edwards et al., 1987). A triple-spike ($^{229}$Th–$^{233}$U–$^{236}$U) isotope dilution method was employed to correct for instrumental fractionation and determine U-Th isotopic ratios and concentrations. The instrumentation, standardization and half-lives are reported in Cheng et al. (2000) and (2013). All U-Th isotopes were measured on a MasCom multiplier behind the retarding potential quadrupole in the peak-jumping mode. We followed similar procedures of characterizing the multiplier as described in Cheng et al. (2000). Uncertainties in U-Th isotopic data were calculated offline at 2σ level, including corrections for blanks, multiplier dark noise, abundance sensitivity, and contents of the same nuclides in spike solution. Corrected $^{230}$Th ages assume the initial $^{230}$Th/$^{232}$Th atomic ratio of 4.4 ±2.2 x$10^{-6}$, the values for a material at secular equilibrium with the bulk earth $^{232}$Th/$^{238}$U value of 3.8.

Cheng, H., Edwards, R. L., Hoff, J., Gallup, C. D., Richards, D. A., Asmerom, Y. 2000. The half-lives of U-234 and Th-230. *Chem. Geol*. **169**, 17–33.

Cheng, H., Edwards, R. L., Shen, C.–C., Polyak, V. J., Asmerom, Y., Woodhead, J., Hellstrom, J., Wang, Y., Kong, X., Spötl, C., Wang, X., Calvin Alexander, E. 2013. Improvements in $^{230}$Th dating, $^{230}$Th and $^{234}$U half-life values, and U–Th isotopic measurements by multi-collector inductively coupled plasma mass spectrometry. *Earth Planet. Sci. Lett.* **371**, 82–91.

Edwards, R. L., Chen, J. H., Wasserburg, G. J. 1987. $^{238}$U, $^{234}$U, $^{230}$Th, $^{232}$Th systematics and the precise measurement of time over the past 500,000 years. *Earth Planet. Sci. Lett*. **81**, 175–192.

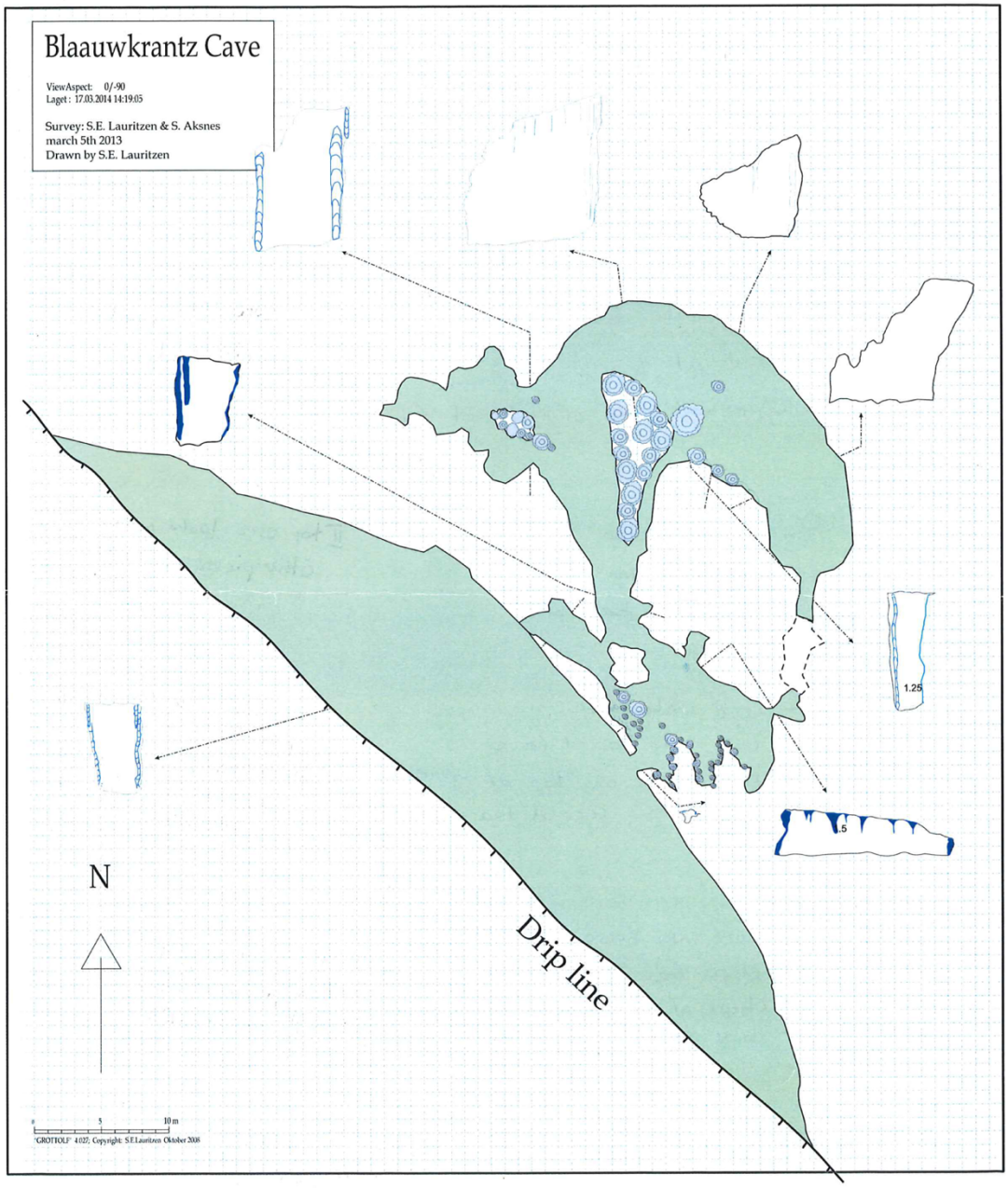


Figure S1: Bloukrantz cave map. A 3D reconstruction of the cave performed by Ole Fredrik Unhammer can be found at : https://sketchfab.com/3d-models/bloukrans-cave-south-africa-600e7347a07a4b26a39bc4eefd5526e2 (Unhammer, O. F., Lauritzen, S.-E., Henshilwood, C. *Photogrammetric mapping of complex cave chambers at Bloukrans Cave, South Africa: Structural, Morphological and Speleogenetic Information*. 26th International Karstological School "Classical Karst" SHOW CAVES AND SCIENCE; 2018-06-18 - 2018-06-22)

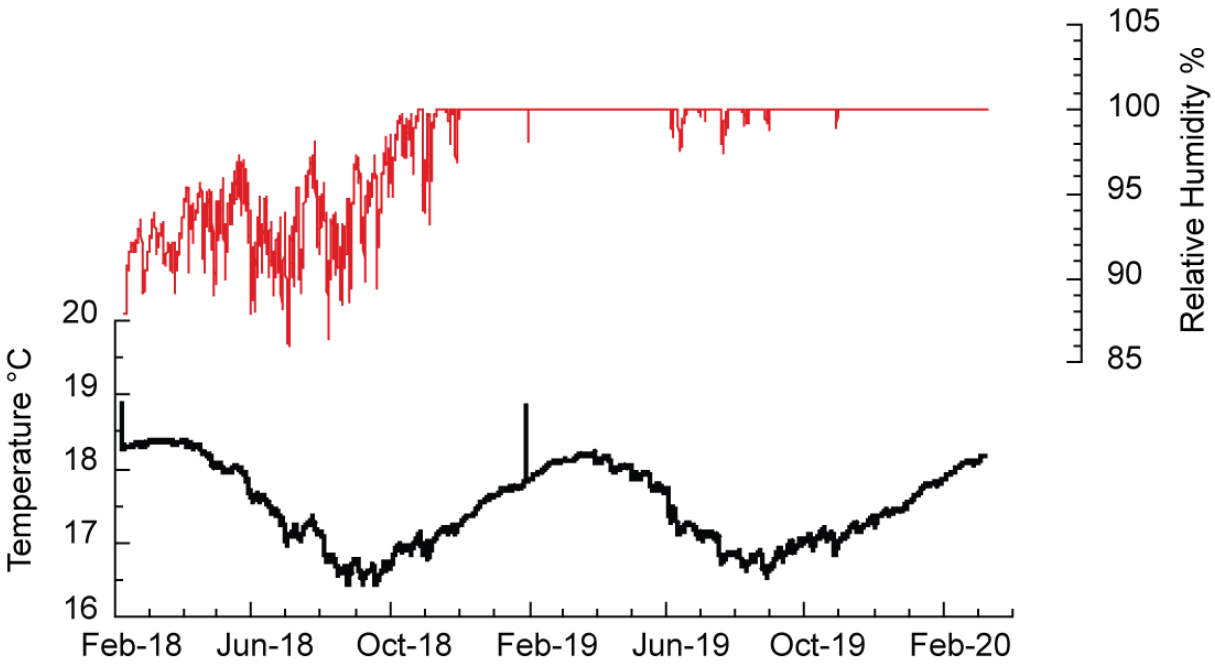


Figure S2: HOBO logger data recorded from February 2018 to March 2020. Top: relative humidity (red); bottom: cave temperature (black).
There was no dripping water observed in February 2018 when the logger was first installed and recorded relative humidity ~90-95%. Dripping was active in January 2019 and March 2020 when relative humidity of 100% were recorded.

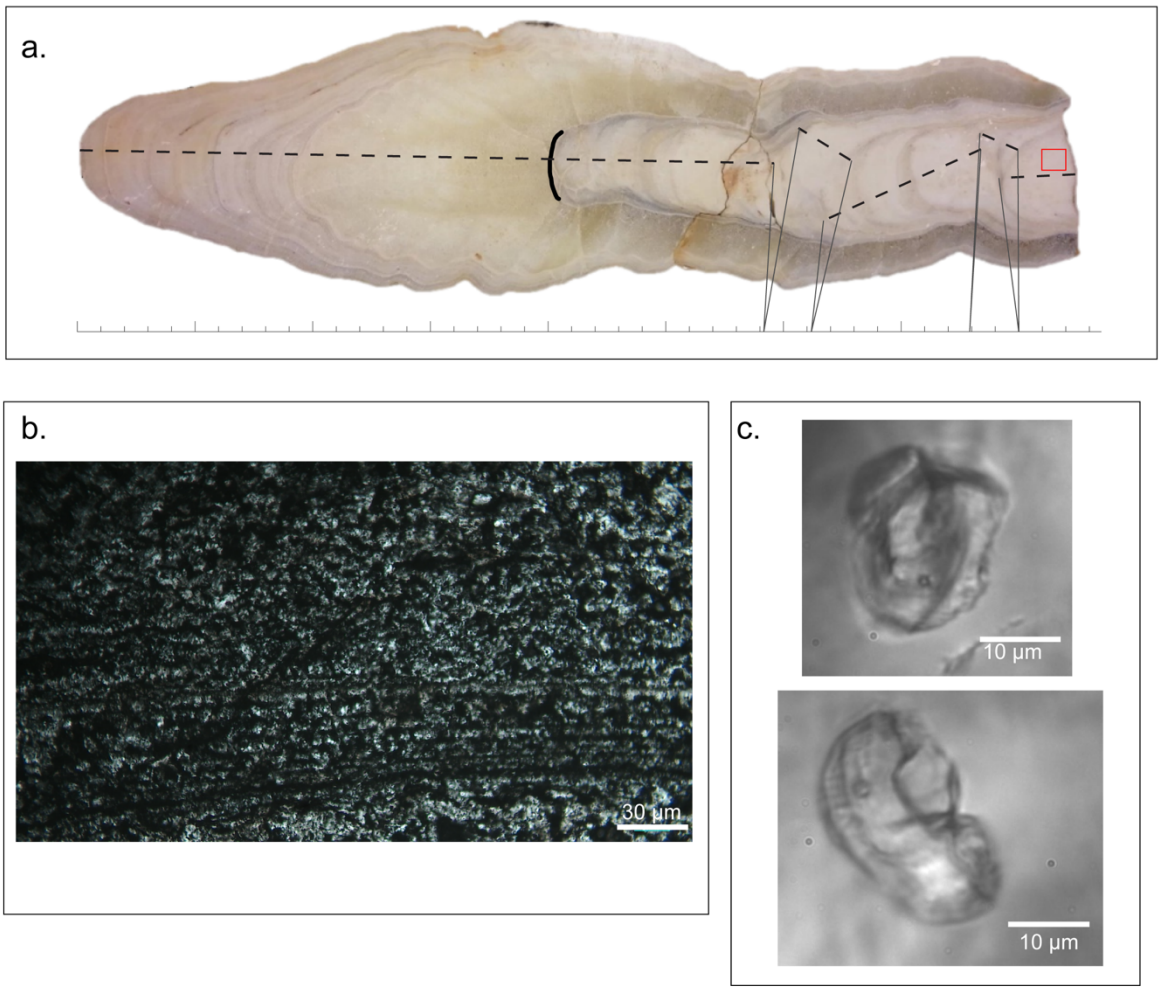


Figure S3: a. Speleothem BL3 from Bloukrantz cave. A hiatus (black line) is visible at mid-length with a change in fabric and color. The red rectangle indicates the approximate location of the thin section shown in b; b. Thin section showing the microcrystalline fabric with a dark layer clearly visible in the lower part; c. Examples of nucleated bubbles in analyzed fluid inclusions.

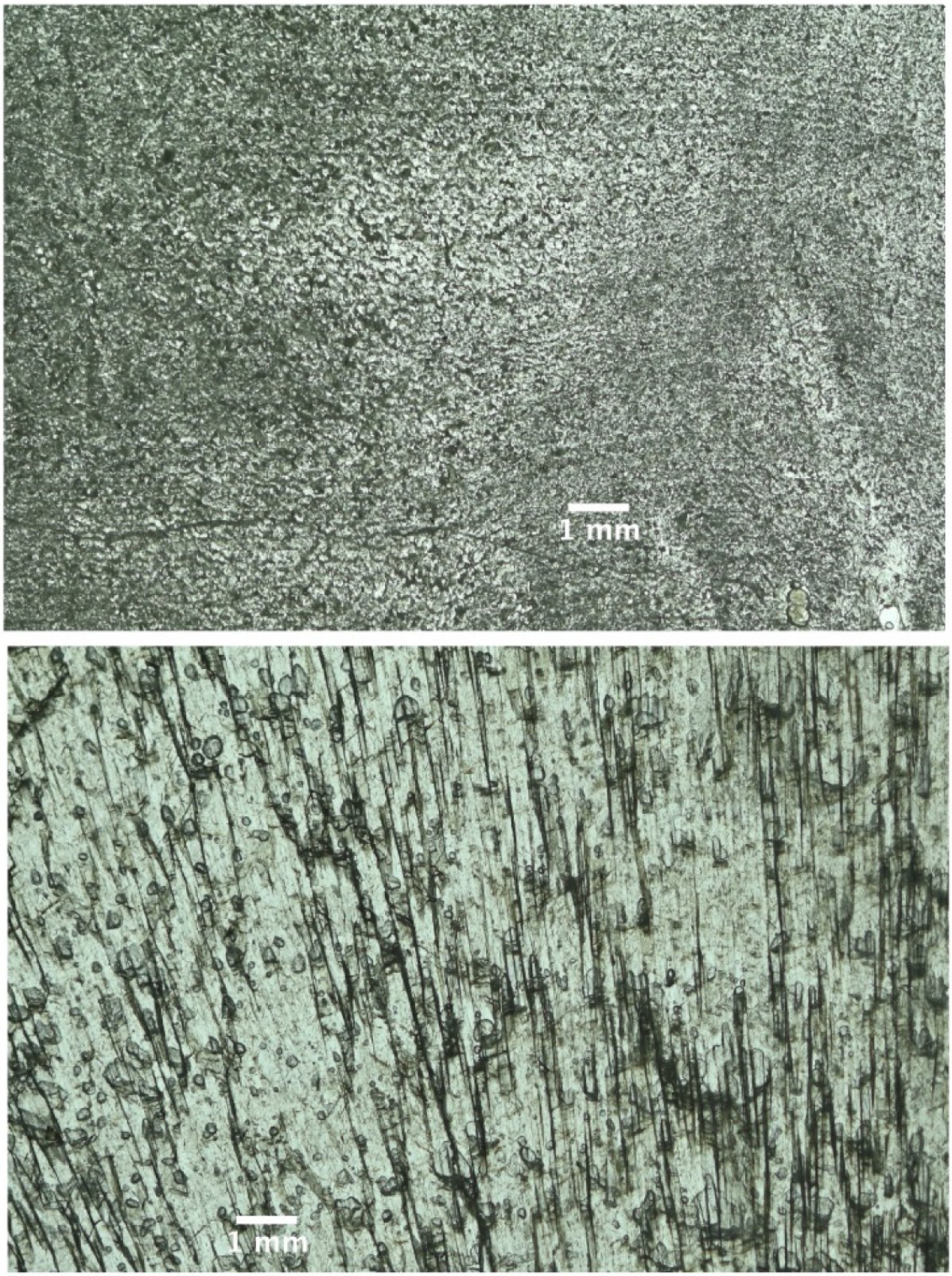


Figure S4: Thin sections illustrating the microcrystalline fabric (top) that characterizes the MIS3 and latest Holocene parts of BL3 and the brittle columnar fabric (bottom) from the early to mid Holocene mentioned in the text (section 2.2).

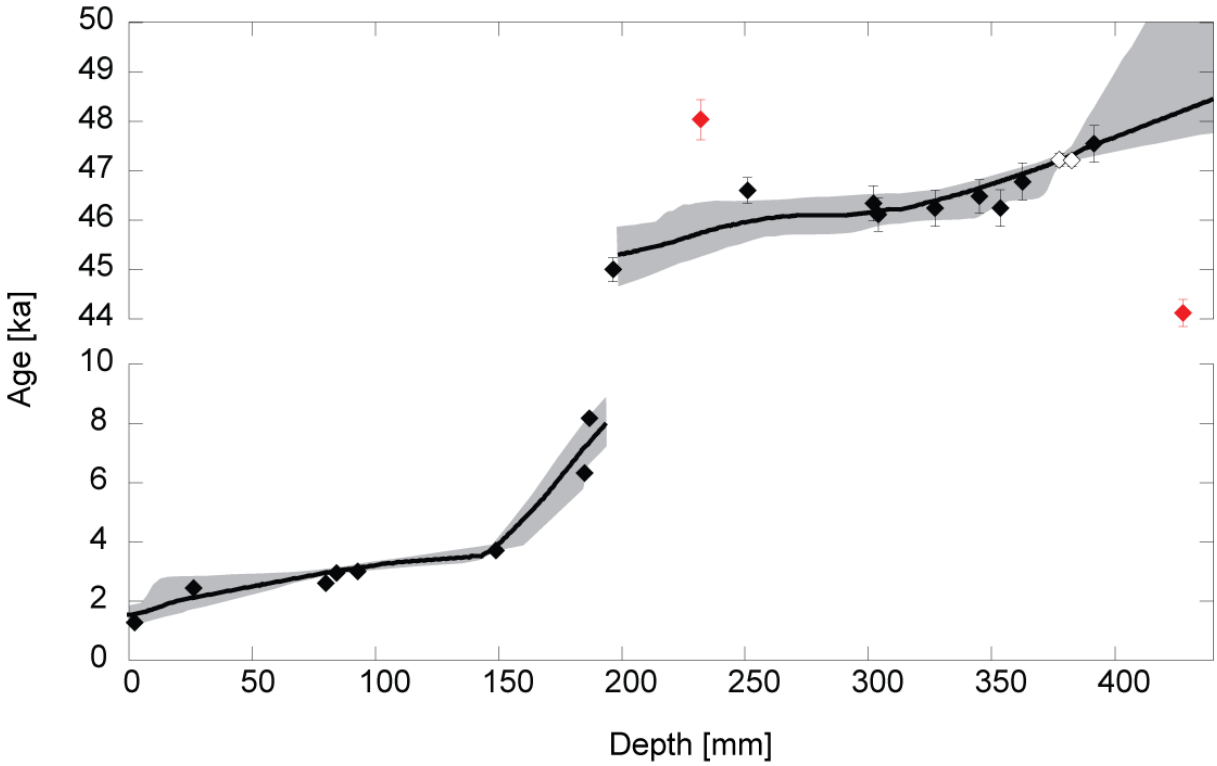


Figure S5: Age model for BL3 using StalAge (Scholz and Hoffmann 2011) and performed as two distinct sections. Grey shading corresponds to 95% confidence interval of the age model. Error bars are shown at 2 sigma level and in some cases are smaller than the symbol size. Red symbols indicate outliers. The two open symbols at ~370 mm correspond to the two samples analyzed at the Isotope Laboratory, Xi'an Jiaotong University.

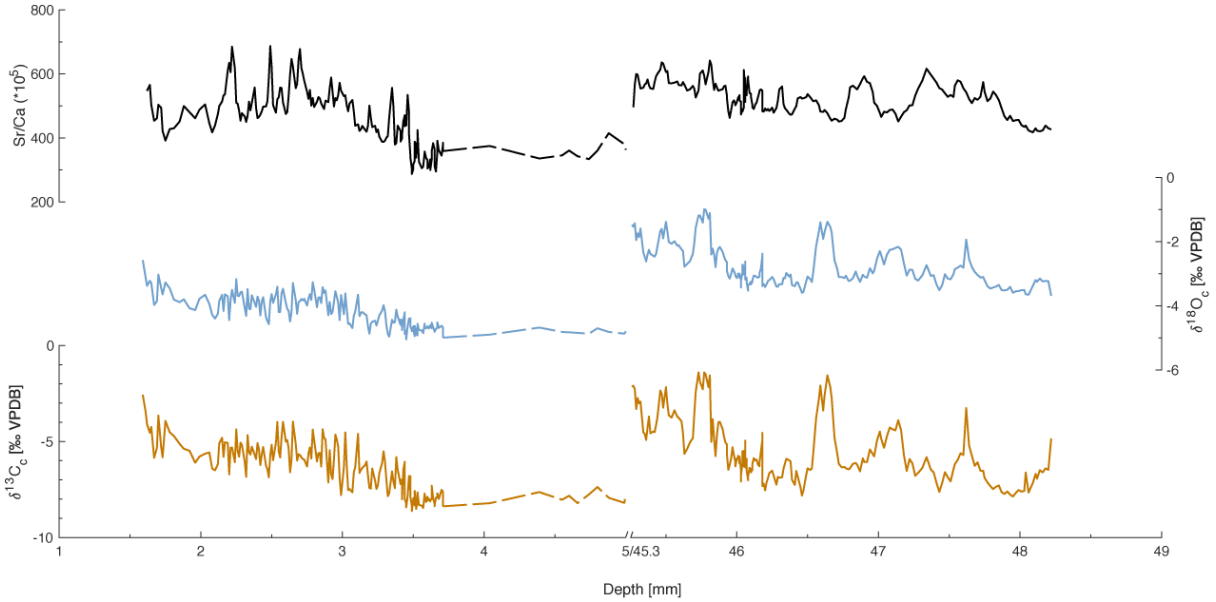


Figure S6: Sr/Ca (black), $\delta^{18}O_c$ (blue) and $\delta^{13}C_c$ (ochre) for the whole stalagmite plotted against age.

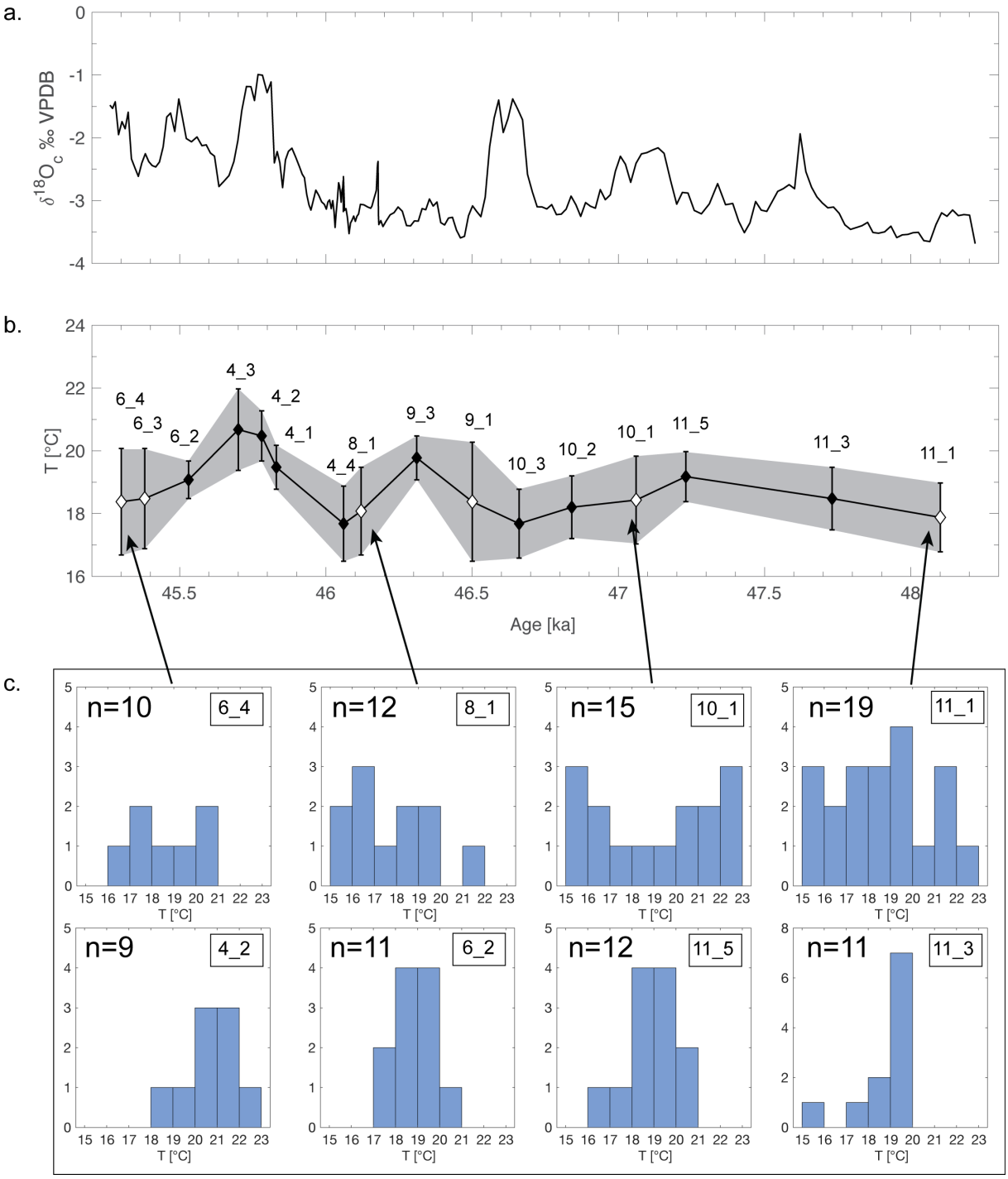


Figure S7:
~~Top.~~ **a.)** $\delta^{18}O_c$. **b.)** Microthermometry temperatures with black symbols representing samples with a 3-6°C range in observed temperatures among the inclusions from the same layer and normal-like distribution, and white symbols representing samples with larger ranges (6-9°C) and more uniform distributions. **c.)** Examples of uniform distribution and large range of the replicate measurements (top row), and normal-like distribution with lower range of the replicate measurements (bottom row).

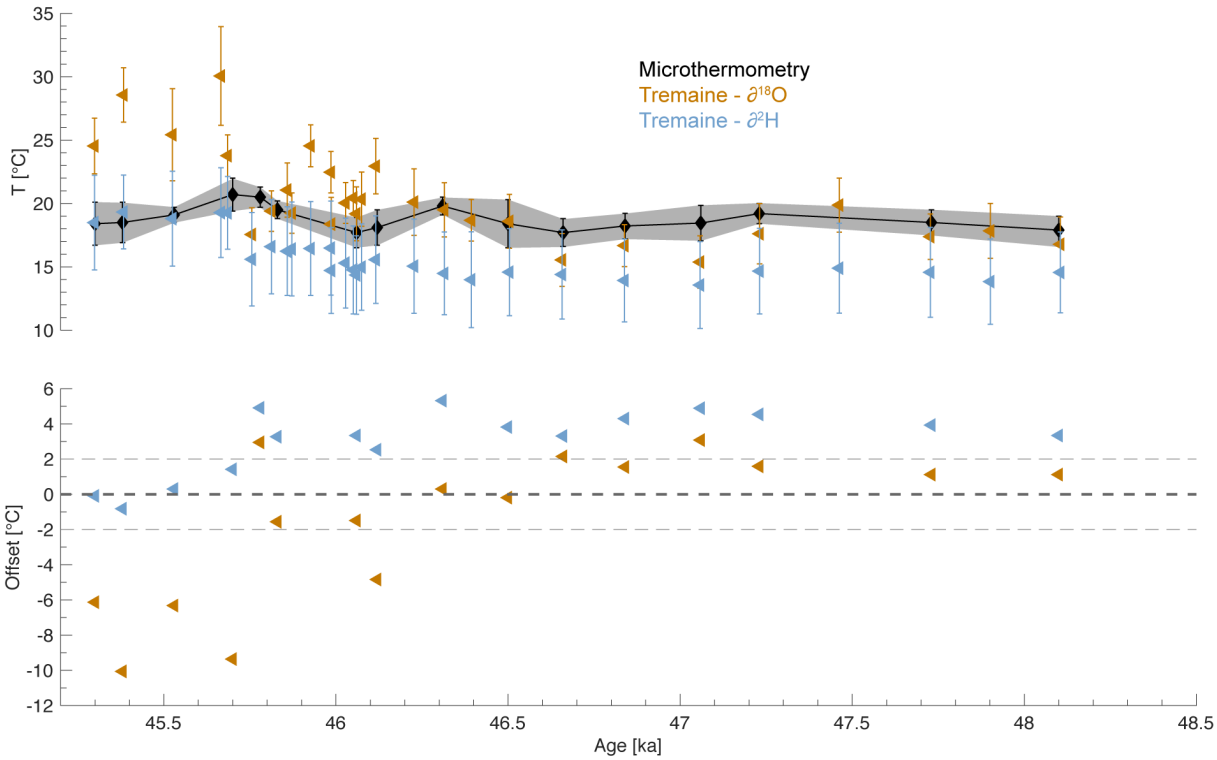


Figure S8: Top: comparison of temperature reconstructions from microthermometry (black diamonds) and FIWI (triangles) using the Tremaine et al. (2011) equation and measured $\delta^{18}O_c$ in combination with either the measured $\delta^{18}O_w$ (ochre) or $\delta^{18}O_w$ inferred from measured $\delta^{2}H_w$ and the local meteoric water line (light blue). The latter calculations give lower temperatures and larger error bars.
Bottom: temperature offset between microthermometry temperature and FIWI temperature calculated with either measured $\delta^{18}O_w$ (ochre) or $\delta^{18}O_w$ inferred from measured $\delta^{2}H_w$ and the local meteoric water line (light blue). Dashed lines indicate the 0 ± 2 °C range. Offsets are systematically higher with inferred $\delta^{18}O_w$ except for the four youngest samples where the estimations from the local meteoric water line show a better agreement with microthermometry.

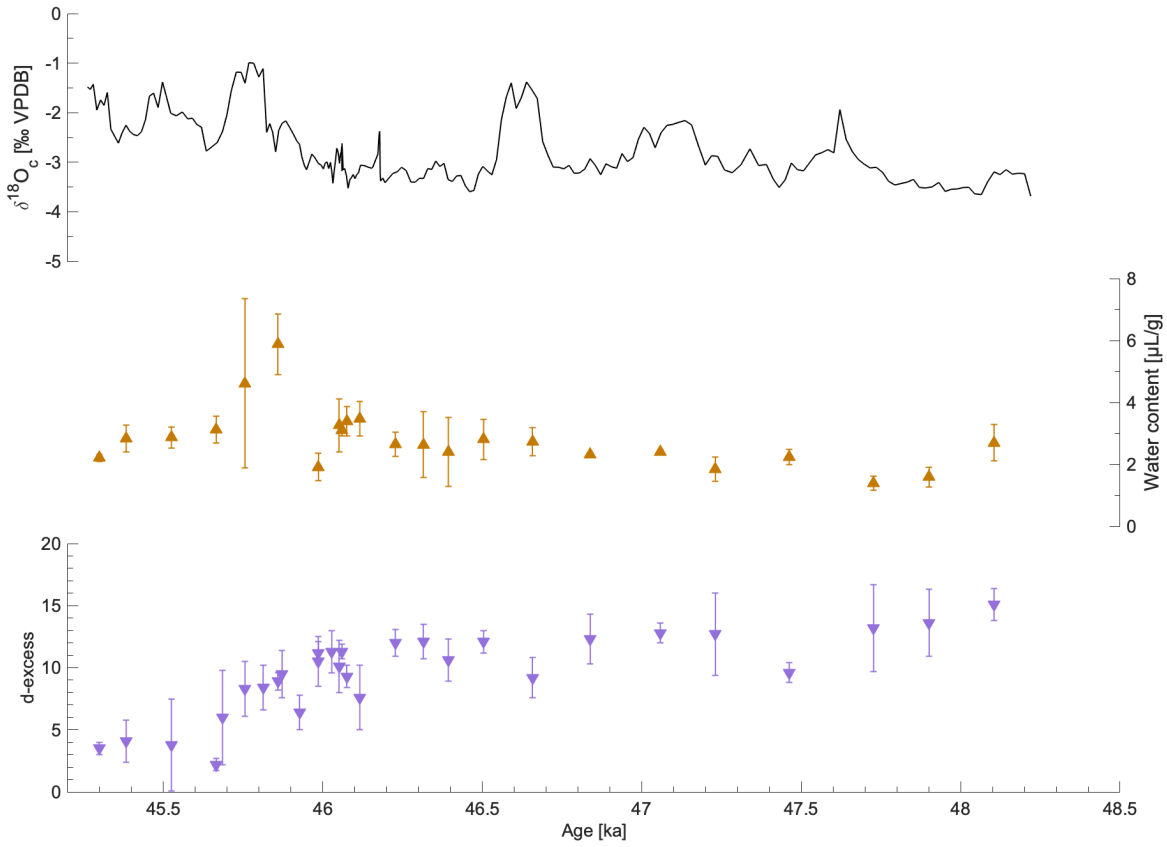


Figure S9: $\delta^{18}O_c$ (top), water content (middle) and d-excess (bottom). The water content is stable throughout the record except for a short increase ~45.8 ka. d-excess values are relatively constant from 48.3 to 46 ka and decrease to lower value from 46 to 45.2 ka.

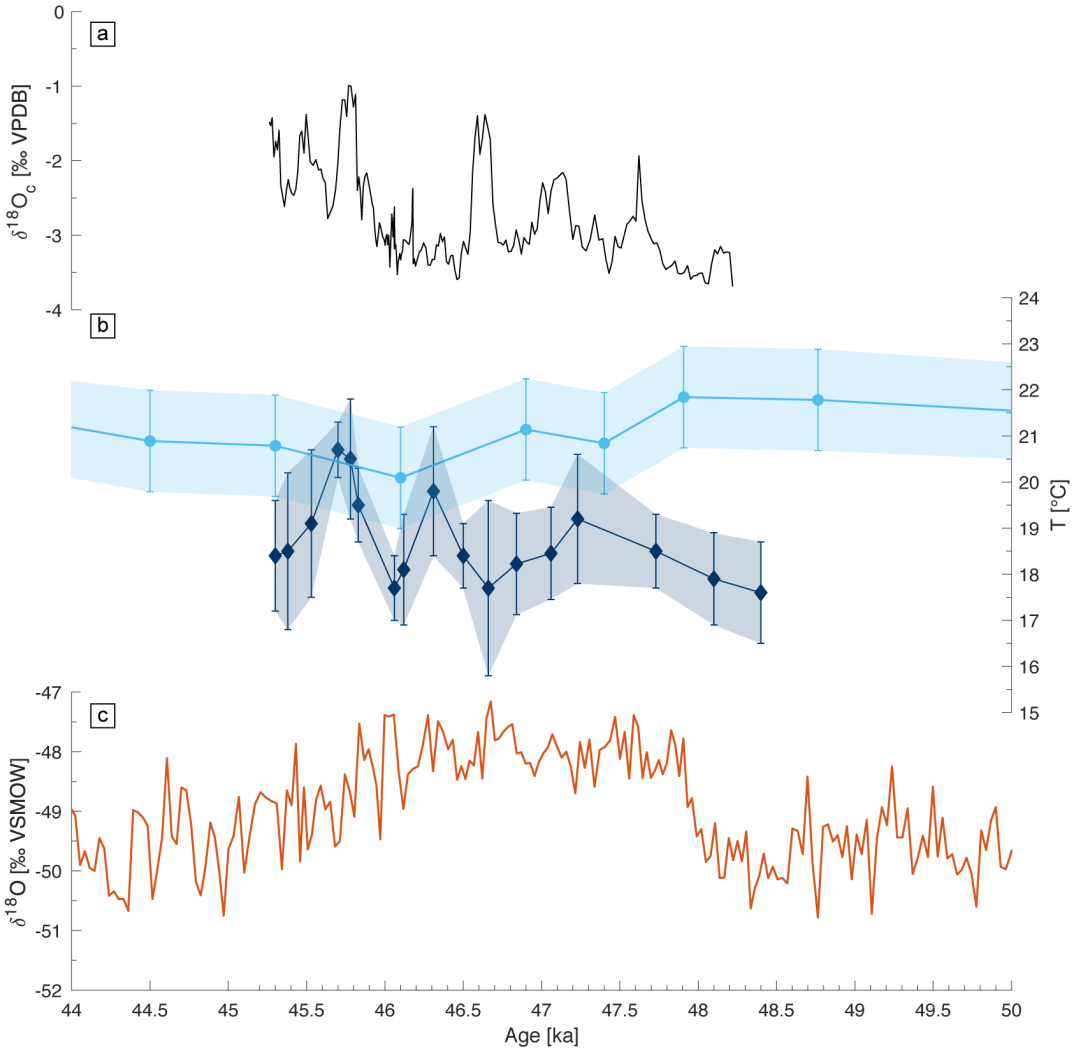


Figure S10: a) $\delta^{18}O_c$ of BL3; b) SST from the Indian Ocean (Simon et al. 2013) and microthermometry data from BL3; c) $\delta^{18}O$ from the EPICA Dronning Maud Land ice core (EPICA community members 2006; EPICA community members 2010).